

Numerical and experimental investigation of a hybrid solar still-solar air heater

Ahmed Ghazy

Mechanical Engineering Department, College of Engineering, Jouf University, Sakaka, Al-Jouf, Saudi Arabia, email: aeghazy@ju.edu.sa

Received 25 July 2022; Accepted 19 January 2023

ABSTRACT

Basin-type solar stills are among the simplest and least expensive solar distillation technologies for transforming saline or brackish water into potable water. Extensive research has been conducted to increase the daily distillate yield of solar stills by increasing incident solar radiation, enhancing saline water evaporation, and enhancing vapor condensation. This study presents a novel hybrid solar still-solar air heater (SS-SAH) in which the condensation energy of the solar still is recovered in heating air for space heating, dehydration of industrial products, and crop drying. The thermal performance of the hybrid SS-SAH has been investigated both experimentally and numerically under hot climate conditions. In addition, the impact of various climate and operational conditions on the thermal performance of the hybrid SS-SAH has been explored. Moreover, comparing the thermal performance of the hybrid SS-SAH to that of a conventional solar still of the same size revealed an improvement of 20%. Furthermore, the thermal performance of the hybrid SS-SAH was enhanced under conditions of high solar irradiance, high air mass flow rate, low ambient temperature, low surrounding wind velocity, and low initial saline water mass. For instance, the overall thermal efficiency of the hybrid SS-SAH increased from 42% to 72% when the air mass flow rate was increased from 0.001 to 0.2 kg/s, and distillate water production increased by 50% with the increase in the solar intensity from 950 to 1,150 W/m².

Keywords: Thermal performance; Solar still; Desalination; Solar air heater

1. Introduction

The lack of potable water has become one of the most challenging issues in many arid regions around the world where there are no freshwater bodies or groundwater resources and rainfall is scarce. Today, approximately 2 billion people worldwide lack access to potable water sources and millions more die annually from diseases caused by contaminated drinking water [1]. Desalination of saltwater or brackish water, which is powered by fossil fuels, has been considered as an efficient and reliable method for meeting the rising demand for potable water. However, due to the negative impact of fossil fuels on the environment and human health, solar-driven desalination was adopted as a promising and sustainable solution to meet the growing demand for fresh water,

particularly in arid and rural areas with no access to power resources and with abundant solar radiation.

Solar stills have been one of the simplest and most cost-effective emerging solar desalination technologies in terms of design, construction, operation, and maintenance. However, the most significant drawback of solar still technology is its low daily distillate production, even when exposed to high levels of solar radiation. This issue has promoted a substantial amount of research aimed at improving the thermal performance of solar stills through the exploration of novel solar stills designs and configurations and the investigation of various performance-influencing parameters. For example, Tanaka [2] increased the daily water production of a single-slope basin still by 70%–100% during the winter by augmenting the incident solar radiation on the still with internal and external reflectors. Tiwari et al.

[3] confirmed that single-slope stills perform better in cold climates than double-slope stills, and vice versa in hot climates. Kumar et al. [4] demonstrated numerically that a double-slope double-effect solar still is nearly twice as efficient as a single-effect solar still. Al-Hinai et al. [5] concluded that, under different design, operational and weather conditions, the average annual water production of the double-effect solar still is about double that of the single-effect solar still. Tayeb [6] disclosed that, of the four stills with different glass cover shapes, the basin still with the inclined flat glass cover produced the most water.

Extensive research has focused on enhancing basin water evaporation. For instance, Omara et al. [7] concluded that the distillate yield of a basin still with a finned base is greater than that with a corrugated base, and that both yields are greater than that of a conventional basin still. Srivastava and Agrawal [8] increased the water production of a basin still by about 68% by including multiple adjacent pieces of blackened jute cloth as floating absorbers on the basin water. By placing sponge cubes in the basin water, Abu-Hijleh and Rababa'h [9] increased the still distillate yield by about 18%–273%. Dumka et al. [10] increased the water distillate of the still by 64% by putting hollow balls of a jute cloth in the basin. Abdel-Rehim and Lasheen [11] increased the efficiency of a basin still by about 5% in the summer by incorporating a PV-driven rotating shaft into the basin water to enhance water vaporization. Essa et al. [12] increased the daily distillate output of a basin still by 124% by affixing two corrugated-surface rotating discs with a wick material to the back wall of the still. Taamneh and Taamneh [13] increased the daily distillate yield of a pyramid-shaped basin still by about 25% by installing a PV-powered fan in the glass cover. By utilizing black granite gravel as an energy storage material, Sakthivel and Shanmugasundaram [14] increased the water production of basin solar still by about 20%. Mevada et al. [15] increased the daily distillate of a single slope still by 76% by incorporating different heat-storing materials into the basin. By adding phase change material (PCM) to the basin, El-Sebaei et al. [16] increased the water productivity of basin solar still during the summer by about 80%, and Katekar and Deshmukh [17] revealed that using paraffin wax as a PCM can increase the productivity of basin stills by 180%. Tabrizi and Sharak [18] integrated a sandy heat reservoir into the basin, which increased the still water productivity on cloudy days and at night.

Enhancing the condensation of water vapor within the stills was yet another means of improving the thermal performance of basin stills. In this context, Arunkumar et al. [19] increased the daily water productivity and efficiency of a basin still with a transparent acrylic hemispherical cover by cooling its cover with water flow. Bapeshwararao et al. [20] concluded numerically that cooling the glass cover of double basin solar still with water flow will increase the distillate in the upper basin, while having almost no effect on the lower basin. Suneesh et al. [21] used cotton gauze to evenly distribute cooling water over the glass cover of the v-type basin still, which increased the daily water distillate in comparison to the conventional method of cooling the glass cover by water flow. Ahmed and Alfaylakawi [22] increased the water production of a basin still by about

30% by frequently sprinkling water on the still's glass cover. Al-Garni [23] increased the summer distillate yield of a single-slope basin still by about 10% and the winter distillate yield of a double-slope basin still by about 8% [24] by using an external fan to cool the glass cover of the still.

El-Bahi and Inan [25] attached an external condenser to a basin solar still to improve water vapor condensation and incorporated an external reflector to increase incident solar radiation, which increased the distillate yield and efficiency of the still to about 7 kg/m²/d and 75%, respectively, during the summer. Fath and Hosny [26] modified the single-slope basin still by tilting the back wall of the still so that it was always in the shade and served as a condenser. Husham Ahmed [27] attached passive cylindrical condensers to the back of basin-type solar stills. The study revealed that the greater the number of cylindrical condensers attached to a still, the greater the distillate yield compared to a conventional basin still. Al-Hamadani and Shukla [28] and Fath [29] employed a second effect still as a separate condenser in the shade of a basin still to increase the condensation and recover condensation energy in a second effect distillation. In addition, numerous double- [30,31] and triple-basins [32] stills have been reported in the literature.

The inevitable condensation energy of the still can be recovered by heating air passing over the glass cover of the still. The resultant heated air can therefore be used for space heating, dehydration of industrial products, and drying of crops such as vegetables, fruits, grains, spices, medicinal plants, tea, coffee, tobacco, etc. This method involves incorporating a glass air heater into the still's glass cover to create a hybrid solar still-solar air heater (SS-SAH). As a result of enhancing solar irradiance harvesting, it is anticipated that the thermal performance the resultant SS-SAH will be better compared to that of the solar still, even though the distillate yield of the still will not increase.

In this paper, a hybrid solar still-solar air heater (SS-SAH) has been locally manufactured and tested in Sakaka (29.9° N, 39.8° E), Saudi Arabia, under its climate conditions. The transient performance of the SS-SAH has been modeled numerically and compared to experimental data. In addition, the transient performance of the SS-SAH was compared to that of a conventional basin-type solar still (CSS) with the same basin area and under the same climate conditions. Moreover, a parametric study for the effects of various design, operational, and climate conditions on the performance of the SS-SAH has been conducted.

2. Theoretical model

Fig. 1 depicts a schematic diagram of the hybrid SS-SAH. The majority of the incident solar radiation is transmitted through the two layers of the glass air heater to the basin of the still. The upper layer (g_2) of the glass air heater absorbs a small portion of the incident solar radiation and reflects a small portion to the ambient surroundings. In addition, the upper glass layer (g_2) of the glass air heater receives thermal radiation from the lower layer (g_1). The energy stored in the upper glass layer (g_2) is then transferred to the circulating air within the glass air heater via convection heat transfer and as convection and radiation losses to the surrounding environment.

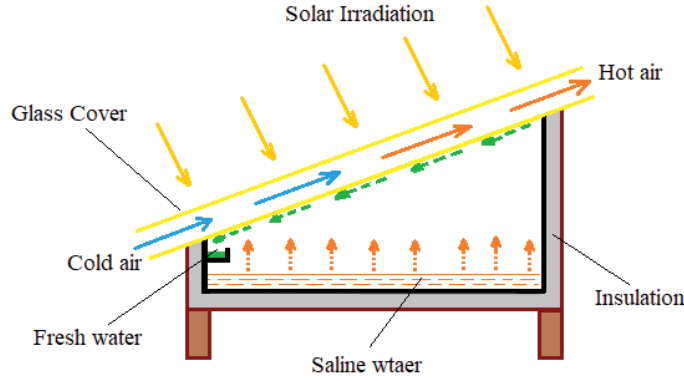


Fig. 1. Schematic diagram and experimental setup of the SS-SAH.

The energy equation for the upper layer (g_2) of the glass air heater is written as follows.

$$m_{g_2} C_{g_2} \frac{dT_{g_2}}{dt} = S_{g_2} + Q_{R,g_1-g_2} - Q_{C,g_2-a} - Q_{R,g_2-sky} - Q_{C,g_2-amb} \quad (1)$$

where

$$S_{g_2} = \alpha_{g_2} I A_{g_2}$$

$$Q_{R,g_1-g_2} = \frac{\sigma A_{g_2} (T_{g_1}^4 - T_{g_2}^4)}{\frac{1}{\epsilon_{g_1}} + \frac{1}{\epsilon_{g_2}} - 1}$$

$$Q_{C,g_2-a} = h_{g_2-a} A_{g_2} (T_{g_2} - T_a)$$

$$Q_{R,g_2-sky} = \sigma \epsilon_{g_2} A_{g_2} (T_{g_2}^4 - T_{sky}^4)$$

$$Q_{C,g_2-amb} = h_{g_2-amb} A_{g_2} (T_{g_2} - T_{amb})$$

The lower glass air heater layer (g_1) of the stores a portion of the incident solar radiation, receives thermal radiation directly from the saline water in the still's basin, and receives thermal energy from the saline water via convection and evaporation through the air within the still. However, it releases thermal energy via convection to the flowing air inside the glass air heater and via radiation to the upper glass layer (g_2). The energy equation for the lower layer of the glass air heater (g_1) is written as follows.

$$m_{g_1} C_{g_1} \frac{dT_{g_1}}{dt} = S_{g_1} + Q_{R,sw-g_1} + Q_{C,sw-g_1} + Q_{e,sw-g_1} - Q_{C,g_1-a} - Q_{R,g_1-g_2} \quad (2)$$

where

$$S_{g_1} = \tau_{g_2} \alpha_{g_1} I A_{g_1}$$

$$Q_{R,sw-g_1} = \sigma \epsilon_{sw} F A_b (T_{sw}^4 - T_{g_1}^4)$$

$$Q_{C,sw-g_1} = h_{sw-g_1} A_b (T_{sw} - T_{g_1})$$

$$Q_{e,sw-g_1} = h_e A_b (P_{sw} - P_{g_1})$$

$$Q_{C,g_1-a} = h_{g_1-a} A_{g_1} (T_{g_1} - T_a)$$

Air circulating within the glass air heater receives thermal energy via convection from both the upper (g_2) and lower (g_1) layers.

$$m_a C_{p,a} \frac{dT_a}{dt} = Q_{C,g_1-a} + Q_{C,g_2-a} \quad (3)$$

The saline water in the still's basin absorbs a portion of the transmitted solar radiation through the glass air heater and receives thermal energy from the basin via convection, while it releases thermal energy directly to the lower glass layer (g_1) via thermal radiation and through the air within the still via convection and evaporation. The energy equation of the saline water is expressed as follows:

$$m_{sw} C_{sw} \frac{dT_{sw}}{dt} = S_{sw} + Q_{C,b-sw} - Q_{C,sw-g_1} - Q_{e,sw-g_1} - Q_{R,sw-g_1} \quad (4)$$

where

$$S_{sw} = \tau_{g_2} \tau_{g_1} \alpha_{sw} I A_b$$

$$Q_{C,b-sw} = h_{b-sw} A_b (T_b - T_{sw})$$

and the variation in the saline water mass during the day was accounted for by the equation.

$$m_{sw} = m_{sw,o} - m_{yield} \quad (5)$$

The basin absorbs the transmitted solar radiation through the saline water and releases thermal energy by

convection to the saline water and by conduction to the basin's insulation as follows.

$$m_b C_b \frac{dT_b}{dt} = S_b - Q_{C,b-sw} - Q_{Cd,b-i} \quad (6)$$

where

$$S_b = \tau_{g2} \tau_{g1} \tau_{sw} \alpha_b I A_b$$

$$Q_{Cd,b-i} = \frac{2 \frac{k_b \times k_i}{k_b + k_i} A_b (T_b - T_i)}{\frac{L_b + L_i}{2}}$$

Finally, the thermal energy stored in the basin's insulation is then released to the ambient surroundings via convection and radiation heat transfer as follows:

$$m_i C_i \frac{dT_i}{dt} = Q_{Cd,b-i} - Q_{R,i-sky} - Q_{C,i-amb} \quad (7)$$

where

$$Q_{R,i-sky} = \sigma \epsilon_i A_i (T_i^4 - T_{sky}^4)$$

$$Q_{C,i-amb} = h_{i-amb} A_i (T_i - T_{amb})$$

The overall thermal efficiency of the hybrid SS-SAH is calculated as:

$$\eta = \eta_{still} + \eta_{heater} = \frac{\sum_{t=0}^{t=t_{op}} ((m_{yield} \times H) + (m_a \times C_a \times \Delta T_a))}{\sum_{t=0}^{t=t_{sun}} I A} \quad (8)$$

3. Experimental set-up

The experimental setup of the hybrid SS-SAH is shown in Fig. 1. The solar still of the hybrid SS-SAH has a blackened galvanized steel basin with dimensions of 0.5 m × 0.5 m × 0.1 m and a thickness of 3 mm. The basin and side of the still were insulated with an extruded polystyrene insulation board of thickness 0.05 m to minimize thermal losses from the still to the ambient surroundings. The still is covered with a 3 mm thick glass sheet that is tilted 30° to maximize solar irradiation reception. Fresh water distillate condenses on the glass cover of the still and is collected in the distillate bottle outside of the still. The glass air heater of the hybrid SS-SAH consists of two 3 mm thick glass sheets that are separated by 0.05 m, with the lower glass sheet serves as the glass cover of the still. Ambient air flows naturally inside the air heater, where it recovers the condensation energy of the still glass cover; however, the airflow can be augmented with the aid of a DC electric fan.

The experimental data were obtained from sunrise to sunset. The ambient temperature and temperature distributions within the SS-SAH were measured using thermocouples of the K-type with a measuring range of -50°C–400°C, an accuracy of ±1°C, and an error of 2%. The incident solar radiation was measured using a digital pyranometer with a measuring range of 0 to 3,999 W/m², an accuracy of ±10 W/m², and a 3% margin of error. A digital anemometer with a measuring range of 0.1–30 m/s, an accuracy of ±0.1 m/s, and an error of 1% was used to measure the wind speed.

The hourly water distillate was measured using a 1,000 mL measuring jar with a 10 mL resolution.

4. Uncertainty analysis

The uncertainty in the result (w_R) is determined by the uncertainties (w_1, w_2, \dots, w_n) in its independent values (x_1, x_2, \dots, x_n) [33] as follows:

$$w_R = \left[\left(\frac{\partial R}{\partial x_1} w_1 \right)^2 + \left(\frac{\partial R}{\partial x_2} w_2 \right)^2 + \dots + \left(\frac{\partial R}{\partial x_n} w_n \right)^2 \right]^{1/2} \quad (9)$$

Since the thermal efficiency (η) of the SS-SAH is determined by measuring the water distillate (m_{yield}), air mass flow rate (m_a), air temperature difference (ΔT_a), and solar intensity (I), the uncertainty in the thermal efficiency of the SS-SAH is estimated by:

$$w_\eta = \left[\left(\frac{\partial \eta}{\partial m_{yield}} w_{m_{yield}} \right)^2 + \left(\frac{\partial \eta}{\partial m_a} w_{m_a} \right)^2 + \left(\frac{\partial \eta}{\partial \Delta T_a} w_{\Delta T_a} \right)^2 + \left(\frac{\partial \eta}{\partial I} w_I \right)^2 \right]^{1/2} \quad (10)$$

where the uncertainty in air mass flow rate is determined by the uncertainty in air velocity (v_a) measurement as follows:

$$w_{m_a} = \sqrt{\left(\frac{\partial m_a}{\partial v_a} w_{v_a} \right)^2} \quad (11)$$

As a result, the uncertainty in measuring the water distillate and calculating the thermal efficiency of the SS-SAH is 1.33% and 0.88%, respectively.

5. Results and discussion

Experimental data was collected for three consecutive days and the discrepancy in measurements was calculate and added to the experimental data in the form of error bars. Fig. 2 shows the measured weather conditions and their trend lines in Sakaka (29.9° N, 39.3° E), Saudi Arabia at the end of September. Solar intensity reached a peak of about 1,000 W/m² at midday, while the ambient temperature reached a peak of 41°C about 2 h later. The wind velocity fluctuated around an average of 1.5 m/s. The numerical model utilized the measured weather data to simulate the performance of the hybrid SS-SAH.

Fig. 3 compares the measured temperature distribution within the hybrid SS-SAH to the temperature distribution predicted by the numerical model using the measured weather conditions shown in Fig. 2. There is a good correlation between the measured temperatures and those predicted by the model. The temperature of the still basin (T_b) is the highest among the components of the hybrid SS-SAH, while the temperature of the saline water (T_{sw}) is slightly lower than that of the still basin, and the temperature of the basin insulation (T_i) is the lowest. In addition, the

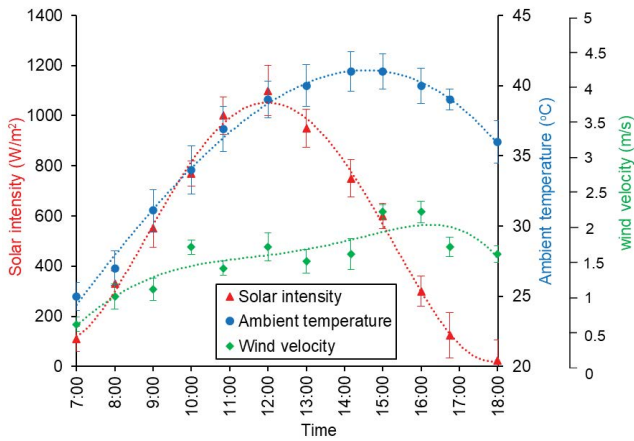


Fig. 2. Measured weather data at Sakaka, Saudi Arabia in September.

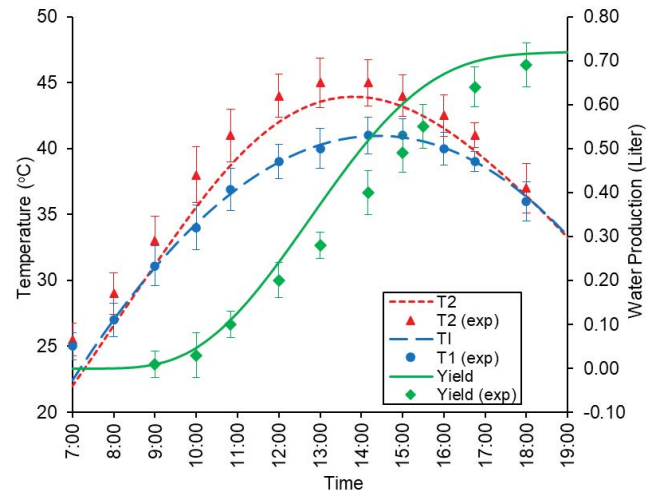


Fig. 4. Distillate water production and air heat gain of the hybrid SS-SAH.

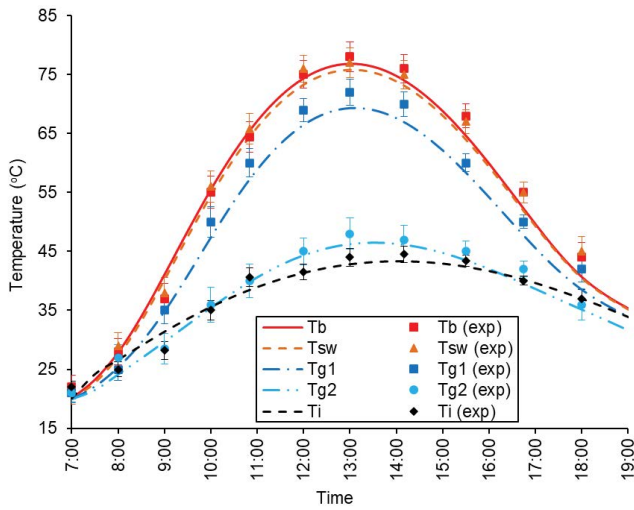


Fig. 3. Theoretical and experimental temperatures distributions within the hybrid SS-SAH.

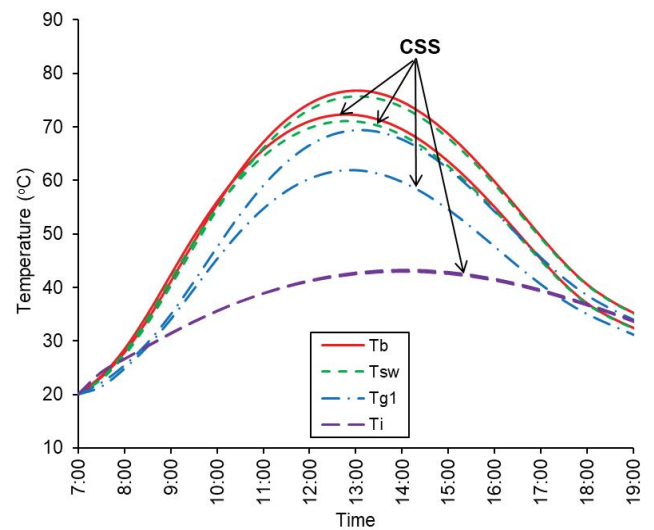


Fig. 5. Temperature distributions within the hybrid SS-SAH as compared to CSS.

temperature of the inner glass cover (T_{g1}) is lower than the temperature of the saline water, which enables the condensation of the fresh water vapor, even though it is markedly higher than the temperature of the outer glass cover (T_{g2}).

The heat gain by the circulating air within the glass air heater is presented in Fig. 4 by the difference in temperature between the entering ambient air temperature (T_1) and the exiting hot air temperature (T_2). In addition, the figure illustrates the accumulated fresh water distillate as well. A daily distillate water production of about 0.7 L/d and a maximum temperature difference of about 5°C across the glass air heater were experimentally measured, which are consistent with the predictions of the numerical model.

The performance of the hybrid SS-SAH was compared to the predicted performance of a conventional single-slope solar still (CSS) of the same size and materials, with the glass air heater of the hybrid SS-SAH replaced with a single-sheet glass cover. The temperature distributions within the hybrid SS-SAH and the CSS are compared in Fig. 5. The hybrid SS-SAH has higher basin, saline water, inner glass cover,

and basin insulation temperatures than does the CSS. This can be attributed to the reduction in the thermal losses from the glass cover to the ambient surroundings in the hybrid SS-SAH as compared to the thermal losses from the CSS.

Consequently, Fig. 6 provides a comparison between the thermal losses from the hybrid SS-SAH and those from the CSS. The thermal loss from the outer glass cover of the hybrid SS-SAH to the ambient surroundings via convection heat transfer ($Q_{(c)g-amb}$) is approximately half that of the CSS glass cover. In addition, the thermal loss via radiation heat transfer is less than that from the glass cover of the CSS. This explains the higher temperature distributions within the hybrid SS-SAH compared to the CSS, as illustrated in Fig. 5.

Fig. 7 shows the overall performance of the hybrid SS-SAH and compares it to that of the CSS. It is demonstrated that the CSS produces 20% more fresh water than the hybrid SS-SAH. However, the overall efficiency of the

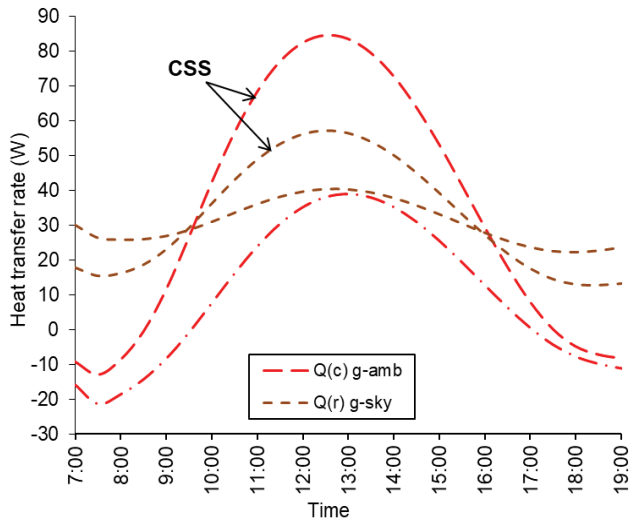


Fig. 6. Thermal losses from the hybrid SS-SAH as compared to the CSS.

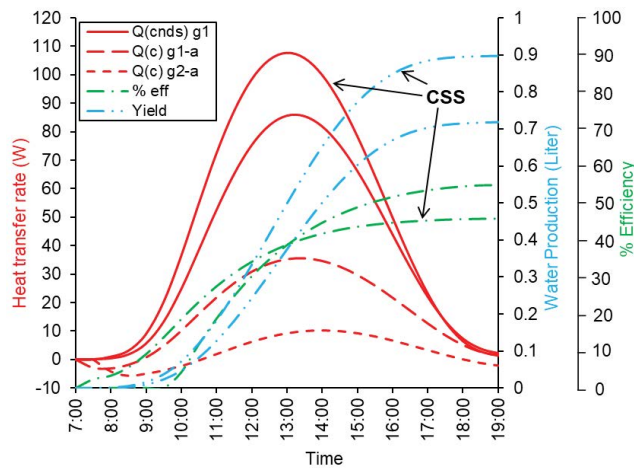


Fig. 7. Overall performance of the hybrid SS-SAH in comparison to that of the CSS.

hybrid SS-SAH is approximately 20% higher than that of the CSS. The reason for this is that the heat gain by the air ($Q_{(c)g1-a}$ and $Q_{(c)g2-a}$) in the glass air heater of the hybrid SS-SAH counterbalances the reduction in its water production.

Fig. 8 shows the influence of the mass flowrate of the circulating air inside the glass air heater of the overall performance of the hybrid SS-SAH. Increasing the air mass flow rate reduced significantly the air's temperature difference. In contrast, the hybrid SS-SAH produced slightly more distillate water as the air mass flow rate increased. Nevertheless, the overall thermal efficiency of the hybrid SS-SAH increased from 42% to 72% by increasing the air mass flow rate from 0.001 to 0.2 kg/s.

The influence of solar intensity on the overall performance of the hybrid SS-SAH over a broad range of air mass flow rates is illustrated in Fig. 9. As the energy input to the hybrid SS-SAH, the increase in irradiance solar intensity increased the heated air temperature difference, the distillate

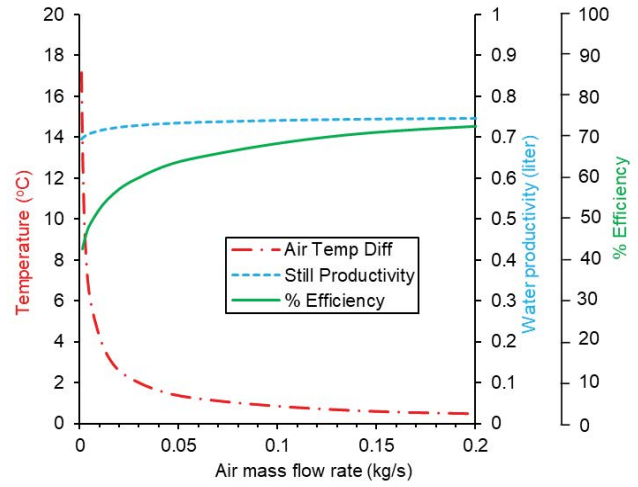


Fig. 8. Impact of air mass flow rate on the performance of the hybrid SS-SAH.

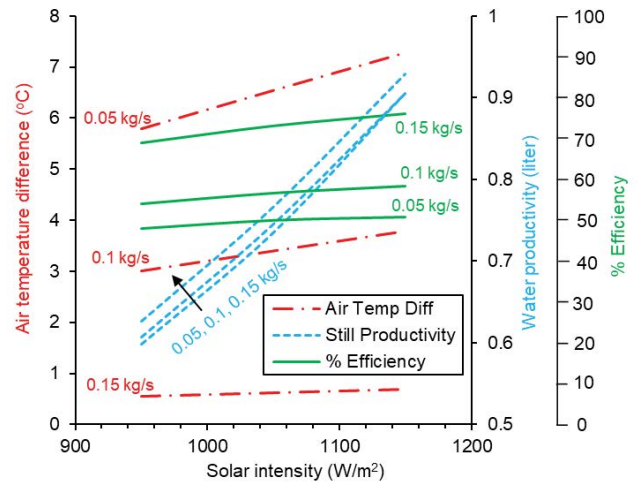


Fig. 9. Effect of solar intensity on the performance of the hybrid SS-SAH for different air mass flow rates.

water production, and the thermal performance at various air mass flow rates. However, the increase in the solar intensity has a noticeable effect on the distillate water production in comparison to other outputs. For instance, an increase in solar intensity from 950 to 1,150 W/m^2 can increase distillate water production by 50%. Furthermore, for various solar intensities, the temperature difference decreased as the air mass flow rate increased, whereas distillate water production and overall thermal efficiency increased, which agrees with the results shown in Fig. 8.

Fig. 10 illustrates the influence of ambient temperature on the overall performance of the hybrid SS-SAH. For various air mass flow rates, any increase in the ambient temperature results in a small increase in the heated air temperature difference, a larger decrease in water distillate production, and a corresponding decrease in the thermal efficiency of the hybrid SS-SAH. This is due to the decreased condensation inside the still as a result to the decreased thermal

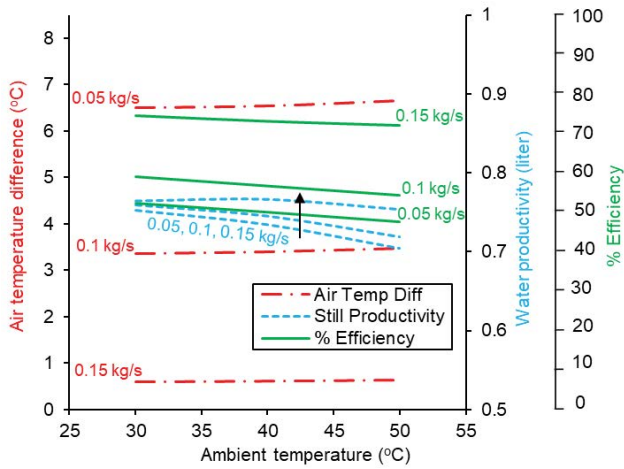


Fig. 10. Effect of ambient temperature on the performance of the hybrid SS-SAH for different air mass flow rates.

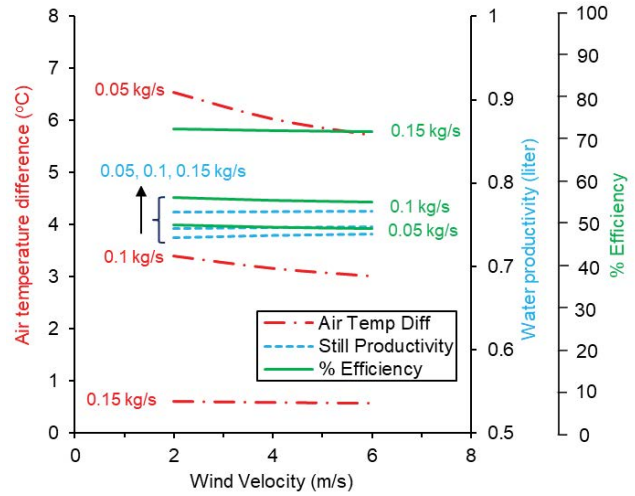


Fig. 12. Effect of wind velocity on the performance of the hybrid SS-SAH for different air mass flow rates.

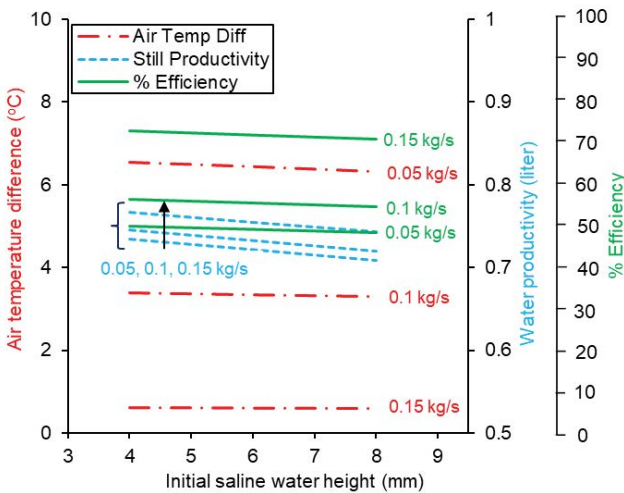


Fig. 11. Effect of initial saline water height on the performance of the hybrid SS-SAH for different air mass flow rates

losses from the glass cover to the surroundings environment. However, for the studied range of ambient temperatures, increasing the air mass flow rate has the typical effect of reducing the heated air temperature difference and boosting the water distillate production and overall thermal efficiency.

Fig. 11 shows the effect of the initial saline water height in the still on the hybrid SS-SAH overall performance. Increasing the initial height of the saline water decreased the flowing air temperature difference, distillate water production, and thus the overall thermal performance of the hybrid SS-SAH for various air mass flow rates. The reason for this is that increasing the initial mass of the saline water reduces water evaporation in the still and, hence, reduces the condensation on the glass cover. In addition, increasing the air mass flow rate has its typical effect on the performance of the hybrid SS-SAH at various saline water heights.

Fig. 12 illustrates the effect of surrounding wind velocity on the performance of the hybrid SS-SAH. The heated air

temperature difference decreased as wind velocity increased for various air mass flow rates, particularly for low air mass flow rates, while distillate water production increased. This is a result of the wind chilling the glass cover. However, the reduction in the air heating outweighs the increase in the distillate water production, resulting in a reduction in the overall thermal performance of the hybrid SS-SAH. In addition, the air mass flow rate has its typical effect on the air temperature difference, distillate water production, and overall thermal efficiency of the hybrid SS-SAH for various wind velocities.

6. Conclusions

A novel hybrid SS-SAH was constructed and tested at Sakaka (29.9° N, 39.8° E), Saudi Arabia. The glass cover of the conventional single-slope solar still has been replaced with a glass air heater in the hybrid SS-SAH to facilitate condensation energy recovery. The hybrid SS-SAH has been modeled numerically and compared to a conventional single-slope solar still of the same size. Although the hybrid SS-SAH produced 20% less fresh water than a conventional solar still, the overall performance of the hybrid SS-SAH was enhanced by 20% as a result of the condensation energy recovery. In addition, the influence of climate and operational conditions on the overall performance of the hybrid SS-SAH has been studied for a wide range of air mass flow rates. The results showed that increasing the air mass flow rate decreased the temperature difference of the heated air while increasing the distillate water production and overall thermal efficiency of the hybrid SS-SAH in various climate and operational conditions. Moreover, the overall thermal efficiency of the hybrid SS-SAH increased as solar intensity increased, but decreased as ambient temperature, wind velocity, and initial saline water height increased. Furthermore, high solar intensity and low initial saline water height increased heated air temperature and distillate water production. However, high ambient temperature and low wind velocity led to an increase in heated air temperature, whereas low ambient temperature and high wind velocity led to an increase in distillate water production.

Acknowledgement

The author extends his appreciation to the Deputyship for Research & Innovation, Ministry of Education in Saudi Arabia for funding this work through the project number “375213500”. The author would like to extend his sincere appreciation to the central laboratory at Jouf University for supporting this study.

Symbols

A	—	Area
C	—	Specific heat
C_p	—	Specific heat at constant pressure
F	—	Radiation view factor
h	—	Heat transfer coefficient
H	—	Latent heat of evaporation
I	—	Solar irradiation
k	—	Thermal conductivity
L	—	Thickness
m	—	Mass
Q	—	Heat transfer rate
S	—	Absorbed solar irradiation
T	—	Temperature
t	—	Time

Greek

Δ	—	Difference
α	—	Surface absorptivity for thermal radiation
ε	—	Surface emissivity for thermal radiation
η	—	Efficiency
σ	—	Stefan–Boltzmann constant
τ	—	Surface transmissivity for thermal radiation

Subscripts

a	—	Circulating air
amb	—	Ambient surroundings
b	—	Still basin
C	—	Convection heat transfer
Cd	—	Conduction heat transfer
e	—	Evaporation
g_1	—	Lower glass layer
g_2	—	Upper glass layer
heater	—	Solar air heater
i	—	Thermal insulation
k	—	Thermal conductivity
o	—	Initial state
op	—	Operation duration
R	—	Radiation heat transfer
sky	—	Sky
still	—	Solar still
sun	—	day duration
sw	—	Saline water
yield	—	Distillate water production

References

[1] R. Wyman, G. Yao, Water, Food, and the Environment, J.M.H. Selendy, Ed., Water and Sanitation – Related Diseases

Water and the Changing Environment, 2nd ed., John Wiley & Sons Inc., UK, 2019, pp. 39–51.

[2] H. Tanaka, Experimental study of a basin type solar still with internal and external reflectors in winter, *Desalination*, 249 (2009) 130–134.

[3] G.N. Tiwari, K. Mukherjee, K.R. Ashok, Y.P. Yadav, Comparison of various designs of solar stills, *Desalination*, 60 (1986) 191–202.

[4] A. Kumar, J.D. Anand, G.N. Tiwari, Transient analysis of a double slope-double basin solar distiller, *Energy Convers. Manage.*, 31 (1991) 129–139.

[5] H. Al-Hinai, M.S. Al-Nassri, B.A. Jubran, Parametric investigation of a double-effect solar still in comparison with a single-effect solar still, *Desalination*, 150 (2002) 75–83.

[6] A.M. Tayeb, Performance study of some designs of solar still, *Energy Convers. Manage.*, 33 (1992) 889–898.

[7] Z.M. Omara, M.H. Hamed, A.E. Kabeel, Performance of finned and corrugated absorbers solar stills under Egyptian conditions, *Desalination*, 277 (2011) 281–287.

[8] P.K. Srivastava, S.K. Agrawal, Experimental and theoretical analysis of single sloped basin type solar still consisting of multiple low thermal inertia floating porous absorbers, *Desalination*, 311 (2013) 198–205.

[9] B.A. Abu-Hijleh, H.M. Rababa'h, Experimental study of a solar still with sponge cubes in basin, *Energy Convers. Manage.*, 44 (2003) 1411–1418.

[10] P. Dumka, R. Chauhan, D.R. Mishra, Experimental and theoretical evaluation of a conventional solar still augmented with jute covered plastic balls, *J. Energy Storage*, 32 (2020) 101874, doi: 10.1016/j.est.2020.101874.

[11] Z.S. Abdel-Rehima, A. Lasheen, Improving the performance of solar desalination systems, *Renewable Energy*, 30 (2005) 1955–1971.

[12] F.A. Essa, A.S. Abdullah, Z.M. Omara, Rotating discs solar still: new mechanism of desalination, *J. Cleaner Prod.*, 275 (2020) 123200, doi: 10.1016/j.jclepro.2020.123200.

[13] Y. Taamneh, M.M. Taamneh, Performance of pyramid-shaped solar still: experimental study, *Desalination*, 291 (2012) 65–68.

[14] M. Sakthivel, S. Shanmugasundaram, Effect of energy storage medium (black granite gravel) on the performance of a solar still, *Int. J. Energy Res.*, 32 (2008) 68–82.

[15] D. Mevada, H. Panchal, M. Ahmadein, M.E. Zayed, N.A. Alsaleh, J. Djuansjah, E.B. Moustafa, A.H. Elsheikh, K.K. Sadasivuni, Investigation and performance analysis of solar still with energy storage materials: an energy-exergy efficiency analysis, *Case Stud. Therm. Eng.*, 29 (2022) 101687, doi: 10.1016/j.csite.2021.101687.

[16] A.A. El-Sebaei, A.A. Al-Ghamdi, F.S. Al-Hazmi, A.S. Faidah, Thermal performance of a single basin solar still with PCM as a storage medium, *Appl. Energy*, 86 (2009) 1187–1195.

[17] V.P. Katekar, S.S. Deshmukh, A review of the use of phase change materials on performance of solar stills, *J. Energy Storage*, 30 (2020) 101398, doi: 10.1016/j.est.2020.101398.

[18] T.F. Farshchi, S.A. Zolfaghari, Experimental study of an integrated basin solar still with a sandy heat reservoir, *Desalination*, 253 (2010) 195–199.

[19] T. Arunkumar, R. Jayaprakash, D. Denkenberger, A. Amimul, M.S. Okundamiya, K. Sanjay, H. Tanaka, H.S. Aybar, An experimental study on a hemispherical solar still, *Desalination*, 286 (2012) 342–348.

[20] V.S.V. Bapeshwararao, U. Singh, G.N. Tiwari, Transient analysis of double basin solar still, *Energy Convers. Manage.*, 23 (1983) 83–90.

[21] P.U. Suneesh, R. Jayaprakash, T. Arunkumar, D. Denkenberger, Effect of air flow on V type solar still with cotton gauze cooling, *Desalination*, 337 (2014) 1–5.

[22] H.M. Ahmed, K.A. Alfaylakawi, Productivity enhancement of conventional solar stills using water sprinklers and cooling fan, *J. Adv. Sci. Eng. Res.*, 2 (2012) 168–177.

[23] A.Z. Al-Garni, Productivity enhancement of single slope solar still using immersion-type water heater and external cooling fan during summer, *Desal. Water Treat.*, 52 (2014) 6295–6303.

[24] A.Z. Al-Garni, Productivity enhancement of solar still using water heater and cooling fan, *J. Sol. Energy Eng.*, 134 (2012) 031006, doi: 10.1115/1.4005760.

- [25] A. El-Bahi, D. Inan, A solar still with minimum inclination, coupled to an outside condenser, *Desalination*, 123 (1999) 79–83.
- [26] H.E.S. Fath, H.M. Hosny, Thermal performance of a single-sloped basin still with an inherent built-in additional condenser, *Desalination*, 142 (2002) 19–27.
- [27] H.M. Ahmed, Seasonal performance evaluation of solar stills connected to passive external condensers, *Sci. Res. Essays*, 7 (2012) 1444–1460.
- [28] A.A.F. Al-Hamadani, S.K. Shukla, Performance of single slope solar still with solar protected condenser, *Distributed Gener. Altern. Energy J.*, 28 (2013) 6–28.
- [29] H.E.S. Fath, High performance of a simple design, two effect solar distillation unit, *Desalination*, 107 (1996) 223–233.
- [30] K.V. Modi, S.R. Maurya, J.H. Parmar, A.B. Kalsariya, P.B. Panasara, An experimental investigation of the effectiveness of partially and fully submerged metal hollow-fins and jute cloth wick-fins on the performance of a dual-basin single-slope solar still, *Cleaner Eng. Technol.*, 6 (2022) 100392, doi: 10.1016/j.clet.2021.100392.
- [31] D. Shukla, K. Modi, Hybrid solar still as a co-generative system and desalination system – an experimental performance evaluation, *Cleaner Eng. Technol.*, 2 (2021) 100063, doi: 10.1016/j.clet.2021.100063.
- [32] M. Patel, C. Patel, H. Panchal, Performance analysis of conventional triple basin solar still with evacuated heat pipes, corrugated sheets and storage materials, *Groundwater Sustainable Dev.*, 11 (2020) 100387, doi: 10.1016/j.gsd.2020.100387.
- [33] J. Holman, *Experimental Methods for Engineers*, 8th ed., McGraw-Hill Companies, New York, 2012, pp. 60–68.